

Gravitational instability of the primordial plasma: anisotropic evolution of structure seeds

Massimiliano Lattanzi^{a,b}, Nakia Carlevaro^a, Giovanni Montani^{c,a,d}

^a*Dipartimento di Fisica, “Sapienza” Università di Roma, P.le A. Moro 5 (00185), Roma.*

^b*Physics Department, University of Oxford, OX1 3RH Oxford, United Kingdom.*

^c*ENEA - C.R. Frascati (Rome), UTFUS-MAG.*

^d*INFN - Sez. Roma1*

Abstract

We study how the presence of a background magnetic field, of intensity compatible with current observation constraints, affects the linear evolution of cosmological density perturbations at scales below the Hubble radius. The magnetic field provides an additional pressure that can prevent the growth of a given perturbation; however, the magnetic pressure is confined only to the plane orthogonal the field. As a result, the “Jeans length” of the system not only depends on the wavelength of the perturbation but also on its direction, and the perturbation evolution is anisotropic. We derive this result analytically and back it up with direct numerical integration of the relevant ideal magnetohydrodynamics equations during the matter-dominated era. Before recombination, the kinetic pressure dominates and the perturbations evolve in the standard way, whereas after that time the magnetic pressure gets much larger and we observe the anisotropic evolution. We quantify this effect by estimating the eccentricity ϵ of a Gaussian perturbation in coordinate space that was spherically symmetric at recombination. For a galactic-sized perturbation, we find that $\epsilon = 0.7$ at $z = 10$ taking the background magnetic field of order 10^{-9} Gauss.

Keywords: Cosmological perturbations, Cosmological magnetic fields, Structure formation, Magnetohydrodynamics.

1. General Remarks

Our theoretical knowledge of the Universe is based on the Standard Cosmological Model, that provides a convenient framework to satisfactorily explain the majority of cosmological observations, like the anisotropy pattern of the cosmic microwave background (CMB) [1, 2, 3], the large-scale structure of the Universe [4, 5, 6], the Hubble diagram of distant type Ia supernovae [7, 8, 9] and the abundances of light elements [10].

The Standard Cosmological Model relies on the assumption that the Universe, at least at large scales, is highly homogeneous and isotropic, and its geometry is thus described by the Robertson-Walker metric. In fact, the distribution of luminous red galaxies shows that the present Universe is homogeneous on scales greater than ~ 100 Mpc [11], while the isotropy of the CMB itself, which has a black-body distribution at $T = 2.73$ K with temperature fluctuations of order 10^{-5} or less, is an indication of the isotropy of the Universe as a whole and a strong evidence for homogeneity at the time of hydrogen recombination (nearly 400.000 years after the Big Bang, corresponding to a cosmological redshift $z_{\text{rec}} = 1100$). On the other hand, below the “homogeneity scale” of 100 Mpc, the distribution of matter is definitely inhomogeneous. Such a dichotomy between the smoothness in the matter-energy distribution at $z = z_{\text{rec}}$ and the clumpiness of the recent Universe, $z \lesssim 1$ below a certain scale is explained by the mechanism of gravitational instability: the structures we observe today have been formed through the growth of tiny density perturbation seeds, that according to the currently accepted model were created in the early Universe during a phase of inflationary expansion.

The presence of a large scale (*i.e.*, coherent over a Hubble length), strong magnetic field is forbidden by the observed isotropy, as it would naturally single out a preferred spatial direction. However, a background, uniform magnetic field could be present at cosmological scales provided that its intensity is small enough. In particular, upper limits of order $\sim 10^{-9}$ G on the present field intensity have been derived from observations of the CMB temperature anisotropies [12, 13] and of its temperature-polarization correlation [14, 1]¹. Smaller scale fields, on the other hand, could be as strong as 10^{-6} G.

The effects of large-scale magnetic fields on the evolution of cosmological structures have been studied extensively in the literature (for a complete review, see Ref. [16] and references therein), where both Newtonian and general relativistic treatments, the latter often using covariant and gauge-invariant techniques, are present. It is known that, among others, magnetic fields slow down (and possibly prevent) the growth of perturbations and can produce vorticities and shape distortions in the density field [17, 18]. In this paper, our goal is to revisit the issue of the existence of a “magnetic Jeans length” and of its dependence on the direction along which the perturbation propagates, other than to give a realistic estimate of its value in a dark matter-dominated Universe. The presence of a magnetic Jeans length has been discussed in several papers [16, 17, 18, 19, 20] both in a Newtonian and in general relativistic framework (for an analysis of the standard Jeans mechanism in presence of dis-

¹It has been argued (see *e.g.*, [15]) that the limits obtained from the CMB temperature data can be significantly relaxed in the presence of free-streaming neutrinos. However this does not affect the limits from the polarization.

sipative effect see also [21, 22, 23]), but some of the analyses failed to recognize its angular dependence. Here, we present a neat derivation of the relevant instability scales based on the equations of magnetohydrodynamics (MHD) on an expanding Universe. We discuss a simple generalization of the magnetic Jeans length suited for two-fluid systems, and clarify some misunderstandings that are present in the literature. We also show the results of the numerical integration of the coupled MHD and Poisson equations. Finally, we numerically study the distortion introduced in the density field by the anisotropy in the critical length.

The paper is organized as follows. In Sec. 2, we characterize the Universe as a plasma. In Sec. 3, we introduce the basic equations, and in Sec. 4 we carry out the linearization procedure. We derive the existence of the magnetic Jeans length from analytical considerations in Sec. 5, while in Sec. 6 we show some numerical results. Finally, we draw our conclusions in Sec. 7.

2. The plasma features of the pre-recombination Universe

Between the time of e^+e^- annihilation (*i.e.*, for a temperature $T = T_{e^+e^-} \simeq 1 \text{ MeV} \simeq 2 \times 10^{10} \text{ K}$) and the time of hydrogen recombination, roughly corresponding to the last scattering of the CMB ($T = T_{\text{rec}} \simeq 0.25 \text{ eV} \simeq 3000 \text{ K}$), the cosmological fluid can be modeled as a plasma of electrons, positrons and photons. We do not consider here the neutrino component because for $T < 1 \text{ MeV}$ it evolves independently of the other components, and interacts only through gravity. The cosmological baryon-to-photon ratio is extremely small and equal to $n_b/n_\gamma \simeq 6 \times 10^{-10}$, where n_γ and n_b are the photon and baryon number densities, respectively. Both n_b and n_γ evolve with the redshift z according to the relation $n_{b,\gamma}(z) = n_{b,\gamma}^0(1+z)^3$, where $n_b^0 \simeq 2.5 \times 10^{-7} \text{ cm}^{-3}$ and $n_\gamma^0 \simeq 410 \text{ cm}^{-3}$ are their present values. In general, in the following we will use a superscript 0 to denote the present value of a quantity. Most of the baryons in the Universe are in the form of hydrogen nuclei, so that for simplicity we assume $n_b = n_p$ (n_p being the proton number density). Furthermore, n_p is also equal to the electron number density $n_e = n_p$, because of the charge neutrality of the Universe.

A fundamental quantity characterizing a plasma is the Debye length λ_D , namely the length over which electrons screen out electric fields in a plasma. It defines the length scale over which a system can consistently be considered to be a plasma. The Debye length of a hydrogen plasma at temperature T is given by the relation $\lambda_D = \sqrt{T/4\pi n_e e^2}$ (e is the proton charge) and then, using the values given above:

$$\lambda_D = \sqrt{\frac{T}{4\pi n_e e^2}} \simeq 6.9 \text{ cm} \sqrt{\frac{T/\text{K}}{n_e/\text{cm}^{-3}}}. \quad (1)$$

Before recombination, photons, protons and electrons share a common temperature $T = T_\gamma$ that, in the absence of entropy-generating processes, evolves like $T_\gamma(z) = T_\gamma^0(1+z)$, where

$T_\gamma^0 = 2.73 \text{ K}$, and then

$$\lambda_D(z) = \frac{2.3 \times 10^4 \text{ cm}}{(1+z)}. \quad (2)$$

Such a specific dependence on the redshift implies that the co-moving Debye length $\bar{\lambda}_D \equiv \lambda_D(1+z)$ is constant during the cosmological evolution and equal to $\bar{\lambda}_D \simeq 2 \times 10^4 \text{ cm}$.

Plasma effects can be relevant in a system when its physical dimension L is much larger than the Debye length. For the Universe, the relevant length is the Hubble radius $L = l_H \equiv cH^{-1}$, where H is the Hubble parameter. This length represents the maximum scale at which microphysical processes can operate in order to establish the thermodynamical equilibrium. Today, $l_H \simeq 10^{28} \text{ cm}$; during the matter dominated era $l_H \propto (1+z)^{-3/2}$, while in the radiation dominated era $l_H \propto (1+z)^{-2}$. From the analysis of both these scales, it is evident that $l_H \gg \lambda_D$ turns out in the period considered here. This means that the cosmological fluid can be considered as neutral at all scales of cosmological interest. We also note that, under the same hypotheses, the baryonic matter M_D within a Debye sphere is also constant and given by

$$M_D = \frac{4}{3} \pi m_p n_b \lambda_D^3 \simeq 10^{-50} M_\odot, \quad (3)$$

where m_p is the proton mass. This ‘‘Debye mass’’ clearly results to be much smaller than any other of cosmological interest.

Another meaningful index is the so-called plasma parameter N_D , *i.e.*, the number of particles within a Debye sphere:

$$N_D = \frac{4}{3} \pi n_b \lambda_D^3. \quad (4)$$

The dependence of λ_D and n_p on the redshift z implies that also N_D is a constant; in particular, since $N_D \simeq 10^7 \gg 1$, the cosmological fluid results to be a weakly coupled plasma.

In order to provide a complete characterization of the cosmological plasma, we now turn our attention to the plasma dissipative properties. Let us start by analyzing the redshift dependence of the plasma resistivity η . For an electron-proton plasma, this is given by $\eta = m_e \nu_{ei} / n_e e^2$, where m_e is the electron mass and ν_{ei} is the electron-ion-collision frequency. For the case under consideration, ν_{ei} is well approximated by the electron-electron collision frequency ν_{ee} [24], *i.e.*,

$$\nu_{ei} \simeq \nu_{ee} \simeq 2.91 \times 10^{-6} \text{ sec}^{-1} \left(\frac{n_e}{\text{cm}^{-3}} \right) \left(\frac{T}{\text{eV}} \right)^{-3/2} \ln \Lambda_C, \quad (5)$$

where $\ln \Lambda_C$ is the Coulomb logarithm, introduced to quantify the effects that small-angle-diffusion collisions have in the Coulomb scattering. A simple estimate of Λ_C in a plasma is given by $\Lambda_C \simeq 12\pi N_D$, so that for the cosmological fluid, the Coulomb logarithm is $\simeq 20$. Substituting Eq.(5) into the expression for the resistivity given above, we get

$$\eta(z) \simeq 1.6 \times \left(\frac{1+z}{1100} \right)^{-3/2} \text{ Ohm cm}. \quad (6)$$

Close to recombination, *i.e.*, $z = z_{\text{dec}} \simeq 1100$, the cosmological plasma has an electric resistivity equal to $\eta|_{z=z_{\text{dec}}} \simeq 1.6 \text{ Ohm cm}$,

i.e., a conductivity $\simeq 0.6$ Siemens cm^{-1} , a value typical of a semiconductor. In Gaussian units, used in the following, $\eta|_{z=z_{\text{dec}}} = 1.8 \times 10^{-12}$ s.

Let us now focus on the viscous properties of the plasma. The shear viscosity coefficient of matter strongly coupled with radiation can be expressed as [25, 26]

$$\eta_v = \frac{4}{15} a_{SB} T^4 \tau, \quad (7)$$

where $a_{SB} \simeq 5.7 \times 10^{-8} \text{ W K}^{-4} \text{ m}^{-2}$ is the Stefan-Boltzmann constant, while τ denotes the mean collision time between particles and can be estimated as $\tau \simeq (n_\gamma \sigma_T v)^{-1}$ (here, we have introduced $\sigma_T \simeq 6.6 \times 10^{-29} \text{ m}^2$ as the cross section for Thomson scattering, and $v \simeq c$). For a photon gas at equilibrium at temperature T , $n_\gamma \simeq 2.0 \times 10^7 (T/\text{K})^3 \text{ m}^{-3}$ and thus we finally obtain

$$\eta_v(T) \simeq 1.2 \times 10^{-4} \left(\frac{T}{\text{K}} \right) \frac{\text{kg}}{\text{m s}}. \quad (8)$$

The resistivity and viscosity coefficients enter the MHD equations through the diffusion coefficients $\bar{\eta} \equiv \eta c^2 / 4\pi$ and $\bar{\eta}_v \equiv \eta_v / \rho_0$, where ρ_0 is assumed to be the background density of the fluid, taken equal to the cosmological baryon density, $\rho_B \simeq 4.2 \times 10^{-28} (1+z)^3 \text{ kg m}^{-3}$ (corresponding to a density parameter $\Omega_B h^2 = 0.022$). Using this and the relation $T = T^0(1+z)$, we get

$$\bar{\eta}_v \simeq 6.4 \times 10^{17} \text{ m}^2 \text{ s}^{-1} \left(\frac{1+z}{1+z_{\text{rec}}} \right)^{-2}, \quad (9)$$

$$\bar{\eta} \simeq 1.3 \times 10^4 \text{ m}^2 \text{ s}^{-1} \left(\frac{1+z}{1+z_{\text{rec}}} \right)^{-3/2}. \quad (10)$$

The relative magnitude of the viscous and magnetic diffusion rates can be parameterized through the magnetic Prandtl number $Pr_m \equiv \bar{\eta}_v / \bar{\eta}$. Using the expression above for $\bar{\eta}_v$ and $\bar{\eta}$ we get

$$Pr_m \simeq 5.0 \times 10^{13} \left(\frac{1+z}{1+z_{\text{rec}}} \right)^{-1/2}, \quad (11)$$

so that $Pr_m \gg 1$, *i.e.*, viscous diffusion is more important than resistive diffusion, at recombination and indeed always at the redshifts under consideration.

Having discussed the relative importance of viscosity- and resistivity-driven dissipative effects, we now discuss at which scales these effects are relevant. In a magnetized plasma, a useful parameter is the Lundquist number $S \equiv L v_A / \eta$, where L is a typical length scale and v_A is the Alfvén velocity, related to the ambient magnetic field B_0 by $v_A^2 \equiv B_0^2 / 4\pi \rho_0$. The Lundquist number is basically the ratio between the resistive diffusion timescale $\tau = L^2 / \eta$ and the Alfvén crossing timescale $\tau_A = L / v_A$. Assuming for the magnetic field at recombination the value $B_0|_{\text{rec}} \simeq 10^{-3} \text{ G}$ (this corresponds to a present intensity of 10^{-9} G) and, considering again $\rho_0 = \rho_B$, we obtain $v_A \simeq 1.2 \times 10^5 \text{ m/s} [(1+z)/(1+z_{\text{rec}})]^{1/2}$. We thus find

$$S = 2.8 \times 10^{23} \left(\frac{L}{\text{Mpc}} \right) \left(\frac{1+z}{1+z_{\text{rec}}} \right)^2. \quad (12)$$

We also compare τ_A with the viscous diffusion timescale defined as $\tau_v = L^2 / \bar{\eta}_v$. The ratio $S_v \equiv \tau_v / \tau_A$ can be thought as a viscous analogous to the Lundquist number:

$$S_v = 5.7 \times 10^9 \left(\frac{L}{\text{Mpc}} \right) \left(\frac{1+z}{1+z_{\text{rec}}} \right)^2. \quad (13)$$

The baryonic mass (at the average background density) contained in a sphere of radius equal to the length where $S \sim 1$ can be calculated to be $\sim 10^{-51} M_\odot [(1+z)/(1+z_{\text{rec}})]^{-3}$, while the analogous quantity for S_v is $\sim 10^{-10} M_\odot [(1+z)/(1+z_{\text{rec}})]^{-9/2}$. Both mass scales are well below the values of cosmological relevance at the redshifts of interest.

The above considerations can be extended also to redshifts $z < 1100$. After that time most of the protons and electrons in the Universe exist inside the neutral atoms of light elements; however, a small residual ionized fraction $x_e = 2.5 \times 10^{-4}$ survives. The calculations carried on so far can be repeated for this post-recombination plasma, [taking also into account that the baryon temperature scales like $(1+z)^2$] and the results are found to be qualitatively similar.

Concluding, the analyses above show how the following hierarchy among the relevant time scales holds for all mass range and redshifts of interest:

$$\tau_A \ll \tau_v \ll \tau_r, \quad (14)$$

meaning that viscosity always dominates over resistivity, and that both dissipative effects can indeed be neglected when studying the propagation of Alfvén waves. In view of the estimation above, in the following we will regard the cosmological medium as an ideal plasma, implying that its dynamical description will be based on an ideal MHD picture.

3. Basic equations

In this section, we derive the basic equations describing the linear evolution of instabilities in the cosmological fluid, modeled as a magnetized plasma. In this respect, we underline that the full investigation of the perturbative dynamics of the Universe would require a general-relativistic treatment, in order to correlate the matter and geometrical fluctuations. However, as long as one is interested in scales much smaller than the Hubble radius, *i.e.*, $L \ll cH^{-1}$, a Newtonian treatment provides a consistent description of the dynamics. Nonetheless, in this scenario the expansion of the Universe can be accounted as the bulk background motion of the fluid [25, 27, 28].

The starting point of our treatment is the Eulerian set of equations governing the fluid motion, on which one can develop a perturbative theory by adding small fluctuations to the unperturbed cosmological background solution. The zeroth-order dynamics is derived by considering a flat homogeneous and isotropic Universe whose energy density is dominated by non-relativistic matter, and correctly describes the expansion of the Universe. We assume that a background magnetic field is present, whose contribution to the total energy density of the Universe can be considered negligible.

Let us now start by briefly recalling the basic equations of non-relativistic, ideal and single fluid MHD, which govern the plasma motion. The mass conservation and the Newtonian gravitational field are described by the continuity and Poisson equations, the single-fluid dynamics is described by the Euler equation in presence of a magnetic field \mathbf{B} and, finally, the electromagnetic interaction can be summarized by the frozen-in and the Gauss laws. Such equations read

$$\partial_t \rho + \nabla \cdot \rho \mathbf{v} = 0, \quad (15a)$$

$$\nabla^2 \Phi - 4\pi G \rho = 0, \quad (15b)$$

$$\rho \partial_t \mathbf{v} + \rho (\mathbf{v} \cdot \nabla) \mathbf{v} + \nabla P + \rho \nabla \Phi - (\nabla \times \mathbf{B}) \times \mathbf{B} / 4\pi = 0, \quad (15c)$$

$$\partial_t \mathbf{B} - \nabla \times (\mathbf{v} \times \mathbf{B}) = 0, \quad (15d)$$

$$\nabla \cdot \mathbf{B} = 0, \quad (15e)$$

respectively, where ρ is the mass density, \mathbf{v} is the velocity field, Φ is the gravitational potential and G is Newton constant. This system constitutes the base of our perturbative approach.

To derive the zeroth-order dynamics we assume the Robertson-Walker metric, *i.e.*, $ds^2 = dt^2 - a^2(t) d\ell^2$, where $a = a(t)$ represents the cosmological scale factor, and a perfect fluid energy-momentum tensor as the matter source of the gravitational field, *i.e.*, $T_\mu^\nu = \text{diag}[\rho_0, -P_0, -P_0, -P_0]$, with $\rho_0 = \rho_0(t)$. In this scheme, the behavior of the mass density with time is obtained from the energy-momentum conservation-law $T_{0;\nu}^\nu = 0$ and from the Friedmann equation, *i.e.*,

$$\dot{\rho}_0 + 3H(\rho_0 + P_0) = 0, \quad (16)$$

$$\dot{a}^2 + \mathcal{K} - \frac{8}{3}\pi G \rho_0 a^2 = 0, \quad (17)$$

respectively [the dot ($\dot{}$) denotes the total derivative with respect to synchronous time]. Here $H = \dot{a}/a$ is the Hubbe parameter and $\mathcal{K} = \text{const.}$ is the curvature factor.

Setting the matter-dominated Universe equation of state (EoS) $P_0 \sim 0$ ($P_0 \ll \rho_0$) in Eq.(16), the zeroth-order solution of the system (15) turns out to be

$$\rho_0 = \frac{\bar{\rho}}{a^3}, \quad \mathbf{v}_0 = H\mathbf{r}, \quad \mathbf{B}_0 = \frac{\bar{\mathbf{B}}_0}{a^2}, \quad \nabla \Phi_0 = \frac{4}{3}\pi G \rho_0 \mathbf{r}, \quad (18)$$

where $\bar{\rho}$ and $\bar{\mathbf{B}}_0$ are dimensional constants, \mathbf{r} ($r = |\mathbf{r}|$) denotes the radial coordinate vector and, of course, $a(t)$ satisfies Eq.(17). We observe how this non-stationary solution characterizing the background dynamics is not affected by the so-called ‘‘Jeans swindle’’ proper of the static solution [25, 27, 28].

To obtain now the explicit time dependence of the unperturbed quantities involved in the model, we restrict the analysis to the flat case, *i.e.*, $\mathcal{K} = 0$. From the Friedmann equation (17) and using the solution for ρ_0 , one readily obtains

$$a = (6\pi G \bar{\rho})^{1/3} t^{2/3}, \quad (19a)$$

$$\rho_0 = \frac{1}{6\pi G t^2}. \quad (19b)$$

Finally, we recall that the adiabatic sound speed is defined by $v_s = \sqrt{\partial P / \partial \rho}$. For a general specific heat ratio γ , we assume

that the pressure varies as $P = K \rho^\gamma$, so that the speed of sound is given by

$$v_s^2 = \gamma K \rho_0^{\gamma-1} = \frac{\gamma K}{(6\pi G)^{\gamma-1}} t^{-2\gamma+2}. \quad (19c)$$

4. Perturbation scheme

In order to analyze the implications that the physics of an ideal magnetized plasma can have on the structure formation, we will follow the standard perturbation approach. In this respect, we consider small perturbations around the zeroth-order cosmological solution derived above, *i.e.*, we write $\rho = \rho_0 + \rho_1$ (with $\rho_1 \ll \rho_0$) and similarly for the other quantities P , \mathbf{v} , Φ and \mathbf{B} . Substituting the perturbed quantities in Eqs.(15) and keeping only terms up to first order, one gets

$$\partial_t \rho_1 + 3H\rho_1 + H(\mathbf{r} \cdot \nabla)\rho_1 + \rho_0 \nabla \cdot \mathbf{v}_1 = 0 \quad (20a)$$

$$\nabla^2 \Phi_1 - 4\pi G \rho_1 = 0 \quad (20b)$$

$$\partial_t \mathbf{v}_1 + H\mathbf{v}_1 + H(\mathbf{r} \cdot \nabla)\mathbf{v}_1 + v_s^2 \nabla \rho_1 / \rho_0 + \nabla \Phi_1 - (\nabla \times \mathbf{B}_1) \times \mathbf{B}_0 / (4\pi \rho_0) = 0 \quad (20c)$$

$$\partial_t \mathbf{B}_1 + 2H\mathbf{B}_1 + H(\mathbf{r} \cdot \nabla)\mathbf{B}_1 + \mathbf{B}_0(\nabla \cdot \mathbf{v}_1) - (\mathbf{B}_0 \cdot \nabla)\mathbf{v}_1 = 0 \quad (20d)$$

$$\nabla \cdot \mathbf{B}_1 = 0 \quad (20e)$$

where, as already discussed, the pressure and density perturbations have been related through the adiabatic sound speed, *i.e.*, $P_1 = v_s^2 \rho_1$. We are assuming that $B_0^2 / 4\pi \rho_0 = v_A^2 \ll 1$, where $B_0 = |\mathbf{B}_0|$, in order to preserve the isotropy of the background flow.

In the following, we replace \mathbf{B}_1 with the dimensionless magnetic fluctuation $\mathbf{b}_1 \equiv \mathbf{B}_1 / B_0$. Moreover, the analysis of the system above can be simplified by Fourier-transforming the spatial dependence of the involved quantities, *i.e.*, using perturbations in the form of plane waves, taking

$$\phi_1(\mathbf{r}, t) = \tilde{\phi}_1(t) e^{i\mathbf{k} \cdot \mathbf{r}}, \quad (21)$$

where $\phi_1 = \{\rho_1, \mathbf{v}_1, \Phi_1, \mathbf{B}_1\}$ is the generic perturbation variable, and \mathbf{k} is the physical wavenumber scaling as $1/a(t)$. It is convenient to consider also the comoving wavenumber $\mathbf{q} = a\mathbf{k}$, that stays constant during the expansion. The evolution for a given harmonic can be simply obtained by the equations in real space with the substitutions $\phi_1 \rightarrow \tilde{\phi}_1$, $\nabla \rightarrow i\mathbf{k}$ and $\partial_t \rightarrow \partial_t - iH(\mathbf{k} \cdot \mathbf{r})$. In the following, for the sake of simplicity, we will drop the tilde over the Fourier transformed variables. Then, the system (20) reduces to (hats denote unit vectors):

$$\dot{\rho}_1 + 3H\rho_1 + i\rho_0(\mathbf{k} \cdot \mathbf{v}_1) = 0, \quad (22a)$$

$$\dot{\mathbf{v}}_1 + H\mathbf{v}_1 + i \left[\frac{v_s^2}{\rho_0} - \frac{4\pi G}{k^2} \right] \rho_1 \mathbf{k} + i v_A^2 \hat{\mathbf{B}}_0 \times (\mathbf{k} \times \mathbf{b}_1) = 0, \quad (22b)$$

$$\dot{\mathbf{b}}_1 + i \hat{\mathbf{B}}_0(\mathbf{k} \cdot \mathbf{v}_1) - i(\hat{\mathbf{B}}_0 \cdot \mathbf{k})\mathbf{v}_1 = 0, \quad (22c)$$

where we have used the Alfvén velocity $v_A^2 = B_0^2 / (4\pi \rho_0)$, and we have already eliminated Φ_1 by means of the Poisson equation in k -space, *i.e.*, $k^2 \Phi_1 = -4\pi G \rho_1$. It is understood that the constraint $\mathbf{k} \cdot \mathbf{b}_1 = 0$ always hold.

Decomposing now \mathbf{v}_1 in its components \mathbf{v}_1^{\parallel} and \mathbf{v}_1^{\perp} parallel and orthogonal to the direction of \mathbf{q} respectively, *i.e.*, $\mathbf{v}_1 = \mathbf{v}_1^{\parallel} \hat{\mathbf{q}} + \mathbf{v}_1^{\perp}$ (where $\mathbf{v}_1^{\perp} \cdot \hat{\mathbf{q}} = 0$), and introducing the following scalar variables:

$$\delta \equiv \rho_1/\rho_0, \quad \theta \equiv i(\mathbf{k} \cdot \mathbf{v}_1) = ikv_1^{\parallel}, \quad (23a)$$

$$\bar{b} \equiv (\mathbf{b}_1 \cdot \hat{\mathbf{B}}_0), \quad \bar{v} \equiv ik(\mathbf{v}_1^{\perp} \cdot \hat{\mathbf{B}}_0), \quad (23b)$$

we finally get a further simplified system:

$$\dot{\delta} + \theta = 0, \quad (24a)$$

$$\dot{\theta} + 2H\theta - \omega_A^2 \delta - \omega_A^2 \bar{b} = 0, \quad (24b)$$

$$\dot{\bar{b}} + (1 - \mu^2)\theta - \mu\bar{v} = 0, \quad (24c)$$

$$\dot{\bar{v}} + 2H\bar{v} + \mu\omega_A^2 \bar{b} = 0, \quad (24d)$$

where we have defined

$$\mu \equiv \hat{\mathbf{B}}_0 \cdot \hat{\mathbf{q}}, \quad \omega_A^2 \equiv v_A^2 k^2, \quad \omega_0^2 \equiv v_s^2 k^2 - 4\pi G \rho_0, \quad (25)$$

and, of course, $0 \leq \mu \leq 1$. We stress that ω_0^2 is *not* positive defined.

5. Evolution of the density contrast and conditions for collapse

The form (24) of the evolution equations has the advantage that it clearly expresses the relationship between the physical quantities involved, other than being very well suited for numerical integration. Some further analytical insight can however be gained by reducing it to a unique higher order equation for the variable $\delta(t)$.

Considering the case of a matter-dominated Universe, and using the explicit time dependence of the quantities involved in the model in that case, *i.e.*, Eqs.(19), with some algebra one can derive the following fourth-order differential equation for $\delta(t)$:

$$\begin{aligned} & 9t^4 \delta^{(4)} + 60t^3 \delta^{(3)} + [9\Lambda_2 + 76 + 9\Lambda_1 t^{-2\nu}] t^2 \delta^{(2)} + \\ & + [(12\Lambda_2 + 8) + 12\Lambda_1(1 - 3\nu)t^{-2\nu}] t \delta^{(1)} + \\ & + [-6\Lambda_2 \mu^2 + 3\Lambda_1(3\Lambda_2 \mu^2 + 12\nu^2 - 2\nu)t^{-2\nu}] \delta = 0, \end{aligned} \quad (26)$$

where $\delta^{(\ell)}$ denotes the ℓ^{th} derivative of δ with respect to time, and we have defined the following constants:

$$\nu \equiv \gamma - 4/3, \quad \Lambda_1 \equiv v_s^2 k^2 t^{2\gamma-2/3}, \quad \Lambda_2 \equiv \omega_A^2 t^2. \quad (27)$$

We recall that γ is the specific-heat ratio ($P \sim \rho^\gamma$) and that $\gamma \geq 4/3$, *i.e.*, $\nu \geq 0$.

The most general solution of Eq.(26) for δ is found to be the superposition of four independent solutions δ_i ($i = 1, \dots, 4$), given by:

$$\delta_i = A_i t^{x_i} {}_2F_3\left[(a_{1i}, a_{2i}); (b_{1i}, b_{2i}, b_{3i}); -\frac{\Lambda_1 t^{-2\nu}}{4\nu^2}\right], \quad (28)$$

where the A_i 's are arbitrary integration constants, ${}_pF_q[(a_1, \dots, a_p); (b_1, \dots, b_q); z]$ denotes the generalized hypergeometric function of argument z , and

$$x_1 = (-1 + \sqrt{\Delta_-})/6, \quad x_2 = (-1 - \sqrt{\Delta_-})/6, \quad (29a)$$

$$x_3 = (-1 + \sqrt{\Delta_+})/6, \quad x_4 = (-1 - \sqrt{\Delta_+})/6, \quad (29b)$$

$$\Delta_{\pm} = 13 - 18\Lambda_2 \pm 6\sqrt{(3\Lambda_2 - 2)^2 + 24\mu^2\Lambda_2}. \quad (29c)$$

The constant coefficients a and b depend, in general, on ν , Λ_2 , μ and we report their complete expressions in Appendix A.

We are now interested in discussing the asymptotic behavior of the hypergeometric functions in the limit of very small or very large argument, *i.e.*, $\Lambda_1/4\nu^2 t^{2\nu} \gg 1$ or $\ll 1$. As in the non-magnetic case discussed in Ref. [25], we restrict the analysis of the asymptotic behavior to the range $0 \leq \nu \leq 1/3$, *i.e.*, for the standard regime $4/3 \leq \gamma \leq 5/3$.

From the asymptotic expansion of the \mathcal{F} functions in the case of large argument, *i.e.*, $\Lambda_1/4\nu^2 t^{2\nu} \gg 1$, the density contrast always shows a damped oscillating behavior with time. In fact, in this regime corresponding to “large” wavenumbers $k \gg 2\nu/\nu_s t$, it always exists at least one asymptotic solution proportional (apart from the oscillating factor) to positive power of the argument $\Lambda_1/4\nu^2 t^{2\nu}$ (*i.e.*, to negative power in time). Such a leading term depends on the value of ν .

On the other hand, the asymptotic expansion of the solutions (28) in the limit $\Lambda_1/4\nu^2 t^{2\nu} \rightarrow 0$, corresponding to “small” wavenumbers $k \ll 2\nu/\nu_s t$, can be written as

$$\delta_i \sim t^{x_i} + O(\Lambda_1/4\nu^2 t^{2\nu}). \quad (30)$$

In order for the gravitational collapse to occur, at least one of the modes has to be growing, *i.e.*, $x_i > 0$. It is fairly easy to show that x_1 , x_2 and x_4 are always negative, whereas the sign of x_3 depends on μ and Λ_2 . In particular, when $\mu \neq 0$, x_3 is negative regardless of the value of Λ_2 , while when $\mu = 0$, x_3 is positive if $\Lambda_2 < 2/3$. This means that density modes with $k \ll 2\nu/\nu_s t$ always grow outside the plane orthogonal to the magnetic field ($\mu \neq 0$), while on that plane ($\mu = 0$) they are kept stable if $k^2 > 2/3\nu_A^2 t^2$ (so that $\Lambda_2 > 2/3$), *i.e.*, if the magnetic field is strong enough.

Remembering that $\rho_0 = 1/6\pi G t^2$, the condition on the wavenumber related to Λ_1 can be rewritten as:

$$k \geq k_J \equiv \sqrt{\frac{24\pi G \nu^2 \rho_0}{v_s^2}}, \quad (31)$$

that is substantially the same as the usual Jeans condition for gravitational instability. In fact, in the non-magnetic case, (to which our analysis reduces for $\omega_A = 0$) this is the only criterion that separates the growing and the decaying modes [25].

In a similar way, the condition related to Λ_2 can be rewritten as:

$$k \geq k_A \equiv \sqrt{\frac{4\pi G \rho_0}{v_A^2}} = \sqrt{\frac{16\pi^2 G \rho_0^2}{B_0^2}}. \quad (32)$$

Summarizing, we find that the presence of a background magnetic field introduces an anisotropy in the stability criterion. While outside the plane orthogonal to \mathbf{B}_0 , the stability of the perturbations is dictated only by the standard Jeans condition $k \gtrsim k_J$, on that plane the unstable modes are those for which the conditions $k < k_J$ and $k < k_A$ both hold². In other words, if $k_A < k_J$ (basically equivalent to $v_A > v_s$), there are Jeans-unstable modes (those in the window $k_A < k < k_J$) that, in the orthogonal plane, are stabilized by the magnetic pressure. The window of stable modes gets wider for larger values of the ambient magnetic field, as expected. We underline that these results are qualitatively the same as those obtained for a static and uniform background [29]. A similar analysis was carried on by the authors of Ref. [17] obtaining a similar results. However, their derivation contained a mistake when separating the real and imaginary components of the evolution equations [25]. For this reason they find a second-order differential equation instead than the fourth-order one discussed here.

6. Numerical Analysis

In the previous section, we have gained an important insight on the effect of a background magnetic field on the evolution of density perturbations. We now show some results obtained through the direct numerical integration of the differential system (24).

6.1. Preliminaries

We will focus in the period of the cosmological evolution that goes from the onset of matter domination ($z \simeq 3000$) to the time of reionization ($z \simeq 10$). We start from matter domination because, before that time, the growth of density perturbation was slowed down and practically frozen by the rapid expansion of the Universe. In the matter-dominated Universe, $a \propto t^{2/3}$ and $H = 2/3t$. We can ignore the presence of a dark energy component since this is sub-dominant until very recent times. The time period that we consider can be divided into two distinct phases, *i.e.*, before and after the recombination of hydrogen occurring at $z \simeq 1100$. Before recombination, the baryons are completely ionized and they are tightly coupled to photons, so that the total pressure of the fluid is given by radiation pressure. After recombination, most of the protons and electrons are in the form of neutral hydrogen atoms, leaving a small ionized fraction $x_e \simeq 2.5 \times 10^{-4}$. Moreover, photons have decoupled so that the baryon pressure is given just by their kinetic pressure, dropping down by several orders of magnitude with respect to its pre-recombination value.

In view of this, we take the speed of sound of the cosmological fluid before recombination to be [25]

$$v_s^2 = \frac{1}{3} \frac{k_B T_b \sigma}{m_p + k_B T_b \sigma}, \quad (33)$$

²It is easy to verify how the physical meaning of the condition is that the timescale for gravitational collapse $\tau_c \sim L/v_c \sim \sqrt{L^3/GM} \sim \sqrt{1/G\rho_0}$ is much shorter than both the acoustic and Alfvén timescales $\tau_s \sim L/v_s \sim 1/kv_s$ and $\tau_A \sim L/v_A \sim 1/kv_A$.

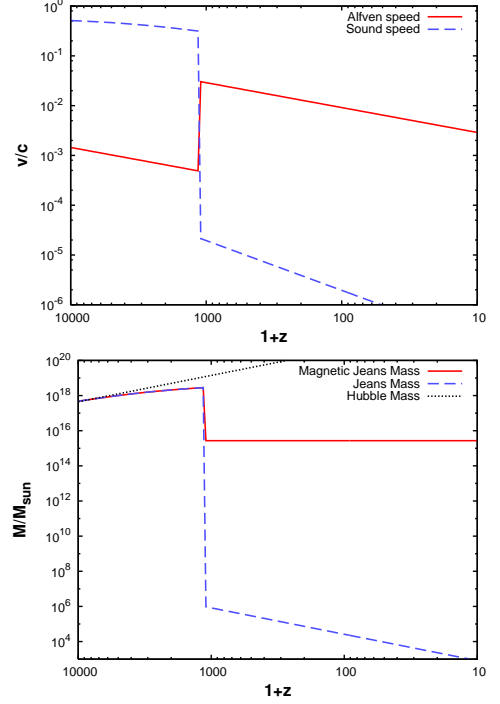


Figure 1: Top panel: Alfvén (red solid line) and sound (blue dashed line) speed as functions of redshift. The discontinuity at $z = 1100$ corresponds to the recombination on neutral hydrogen. Bottom panel: Magnetic (red solid line) and standard (blue dashed line) Jeans mass as a function of redshift. The mass contained inside the Hubble radius (black dotted line) is also shown for comparison.

where $T_b = T_\gamma$ is the common photon-baryon temperature and $\sigma = 4a_{SB}T^3/3n_b k_B \simeq 1.5 \times 10^9$ is the specific entropy. After recombination, we take instead

$$v_s^2 = \frac{5}{3} \frac{k_B T_b}{m_p}, \quad (34)$$

where it should be taken into account that after recombination T_b differs from T_γ and scales like a^{-2} instead than a^{-1} . Finally, unless otherwise stated, in order to calculate the Alfvén speed $v_A = \sqrt{B_0^2/4\pi\rho_0}$ we take a magnetic field with a present day intensity of 10^{-9} Gauss, while the density of charged particles is equal to the total baryon density $\rho_b = n_b m_p$ before recombination, and equal to the ionized density fraction $x_e n_b m_p$ after that time. A plot of the Alfvén and sound speeds as functions of redshift is shown in Figure 1. The sudden drop in the sound speed at recombination is due to the sharp decrease of baryon pressure after photon decoupling, while the equally sudden increase in the Alfvén speed at the same time is due to the decrease in the density of charged particles.

In a detailed model, the presence of different uncoupled components making up the matter content of the Universe should be taken into account. In fact, most of the matter ($\sim 80\%$) is in the form of cold dark matter (CDM), interacting with the baryon-photon fluid only through the gravitational force. Moreover, after recombination, recombined and ionized hydrogen atoms should be effectively treated as distinct fluids, that again are coupled only by gravitation. Thus, a proper treatment should

rely at least on a two- and three-fluid description before and after recombination, respectively. Here, we will make some approximations in order to be able to use the single fluid description and still be able to draw meaningful conclusions about the perturbations in the baryonic component. First of all, we ignore the perturbations in the CDM component, in the pre-recombination era, this is justified by the fact that the large radiation pressure prevents baryons to fall into the potential wells created by CDM; this is known to be true in the non-magnetic case but we expect it to hold also in the case under consideration since, as seen in the last section, the magnetic field only acts to increase stability. After recombination, our treatment will rigorously remain valid for some time, *i.e.*, only as long as the baryon density fluctuations do not catch up with those in the CDM component.

For what concerns the modeling of the gravitational interaction between the neutral and ionized baryon components after recombination, we proceed in the following way. It is reasonable to assume that the newly recombined baryons inherit the fluctuations they had prior to recombination, so that at recombination $\delta_{\text{HI}} = \delta_{\text{HII}}$ (we use standard astronomical notation for ions). The neutral component obeys its own continuity and Euler equations (the latter obviously lacking the Lorentz force term) that are coupled to the corresponding equations for the ions by the Poisson equation, whose perturbed version will read $\nabla^2 \Phi_1 = 4\pi G(\delta\rho_{\text{HI}} + \delta\rho_{\text{HII}})$. Given that the reionization fraction is very small, $\rho_{0,\text{HI}} \gg \rho_{0,\text{HII}}$ and then, since $\delta_{\text{HI}} \simeq \delta_{\text{HII}}$, it is immediate to see that $(\delta\rho_{\text{HI}} + \delta\rho_{\text{HII}}) \simeq \delta\rho_{\text{HI}} \simeq \rho_{0,\text{HI}} \delta_{\text{HII}}$. In other words, the Poisson equation rewrites:

$$\nabla^2 \Phi_1 = 4\pi G \rho_{0,\text{HI}} \delta_{\text{HII}}, \quad (35)$$

so that the fluctuations in the neutral component do not explicitly appear and we have reverted to a one-fluid approximation, although with a different source term for the gravitational field. It is easy to see that the only place where this source appears in the final equations is in the expression for ω_0^2 . Thus we can conclude that the gravitational effect of the neutral component can be taken into account by the simple prescription that the density that appears inside ω_0^2 should always be taken to mean the *total* (*i.e.*, neutral + ionized) density of baryons. We remark again that this approach will be valid only as long as $\delta_{\text{HI}} = \delta_{\text{HII}}$, so that we expect it to cease to provide a proper description some time after recombination.

Before showing the results of the numerical integration, we illustrate in the right panel of Figure 1 the evolution of the standard Jeans wavenumber (31) and of its “magnetic” counterpart (32). Consistently with the discussion above, we use the total baryon density in both expressions, excepted when computing the Alfvén speed, where we have to use the density of the ionized fraction (in other words, barring constants, $k_A^2 \propto \rho_{0,\text{HI}} \rho_{0,\text{HII}} / B_0^2 = x_e \rho_{0,\text{HI}}^2 / B_0^2$). In order to take out the change in k_J and k_A due to the expansion, we follow the convention to express the results in terms of the mass contained inside the corresponding length scales $1/k_{JA}$. In particular, we consider the total baryonic mass (irrespective of the ionization state), contained inside a sphere of radius $2\pi/k_{JA}$. It can be

seen that the window of modes that are made stable by the magnetic field, *i.e.*, those between the red dashed and the black solid line, spans, right after recombination, ten orders of magnitude in mass.

As noted in the introduction, the existence of a magnetic Jeans length has been studied previously and all expressions for the critical wavenumber agree, apart from numerical factors, with expression (32). However, we argue that the numerical estimates of this quantity appearing in the literature are somewhat inaccurate since it is often taken ρ_0 inside the formula to be equal to the present critical density $\rho_c \simeq 9 \times 10^{-27} \text{ kg m}^{-3}$. This yields at the present time a magnetic Jeans length $\lambda_A \sim 1/k_A \sim 10 \text{ kpc}$ for $B_0 = 10^{-9} \text{ G}$ and $\lambda_a \sim 1 \text{ Mpc}$ for $B_0 = 10^{-7}$.³ These values would be accurate if a) the Universe were baryon-dominated, and b) all the baryons were in ionized form, but this situation is never realized in practice. One should instead take into account the actual density of baryons and, after recombination, the fact that only a small fraction is ionized. Following our previous discussion, this is realized by the substitution $\rho_0^2 \rightarrow x_e \rho_{0,\text{HI}}^2$, that yields $\lambda_A \sim 100 (10^4) \text{ Mpc}$ for $B_0 = 10^{-9} (10^{-7}) \text{ G}$ (the latter value being even larger than the present Hubble radius). This approximation holds for a limited time after recombination; once the baryons start to fall into the potential wells created by CDM, the same reasoning leads to the substitution $\rho_0^2 \rightarrow \rho_{0,\text{HII}} \rho_m$ where $\rho_m \simeq 0.135 \rho_c$ is the total matter density. Inserting the numerical values one gets $\lambda_A \sim 40 (4 \times 10^3) \text{ Mpc}$ for $B_0 = 10^{-9} (10^{-7}) \text{ G}$.

6.2. Results

We now discuss the results of the direct numerical integration of Eqs.(24). The initial conditions for the integration have been chosen using the fact that power-law solutions for δ can be found in the limit $t \rightarrow 0$ (because in that limit both ω_A^2 and ω_0^2 are proportional to t^{-2}). There are four distinct solutions of this kind, but only one corresponds to a growing mode. We have matched the initial conditions to the asymptotic growing solution at the initial time of integration. The latter has been chosen so that all the modes of interest were outside the horizon at that time. Even if the initial time falls in what would be the radiation-dominated era, nevertheless we always consider a matter-dominated Universe. All results have been normalized to the initial value of the density contrast.

In Figure 2, we show the evolution of the density contrast for three different wavenumbers $k = (1.7, 0.36, 0.08) \text{ Mpc}^{-1}$ (normalized at the present time), *i.e.*, for the following baryonic masses $M = (1.7 \times 10^{11}, 1.7 \times 10^{13}, 1.7 \times 10^{15}) M_\odot$. These masses roughly correspond to the galactic, cluster and super-cluster mass scales, respectively. For each mode, we show the evolution in both the direction parallel to the background magnetic field ($\mu = 1$) and orthogonally to that direction ($\mu = 0$).

³The latter value is also often said to be of the order of the scale of a galaxy cluster, while in effect it is closer to the scale of a galaxy as it can be seen by the fact that the mass enclosed inside a sphere of 1 Mpc radius at the critical density is $\sim 10^{11} M_\odot$. The reason why a galaxy is much smaller than 1 Mpc is that it has detached from the Hubble flow and undergone non-linear evolution, so that its density is much larger than the cosmological average [27].

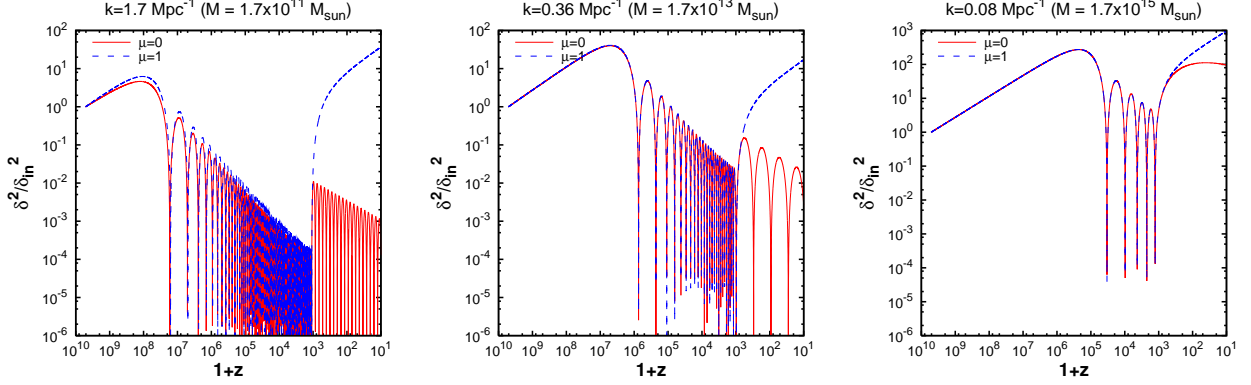


Figure 2: Evolution of the dimensionless density perturbation δ with redshift. The three panels show three different mass scales roughly corresponding, from left to right, to the galaxy, cluster and supercluster scales. In each panel, we show the evolution of perturbations orthogonal (red solid line) and parallel (blue dashed line) to the background magnetic field.

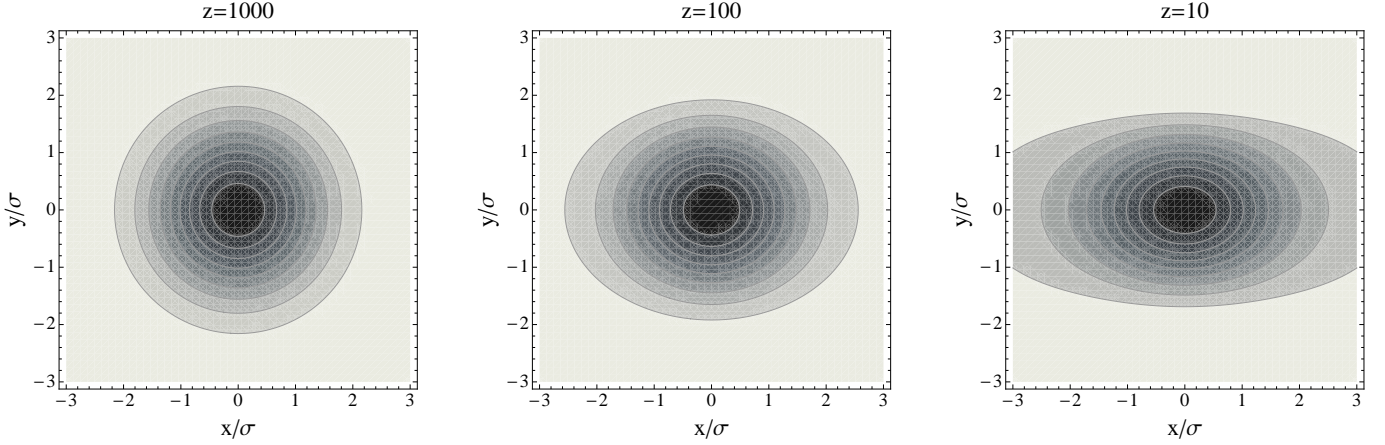


Figure 3: Equal density contours of an initially spherically symmetric Gaussian perturbation at the galactic scale in the x - y plane, at different times. The contours correspond to $(0.1, 0.2, \dots, 0.9)$ times the central density. The background magnetic field is directed along the y axis and has an intensity $B_0 = 10^{-9}$ G.

The present-day strength of the field is $B_0 = 10^{-9}$ G. In all cases, the perturbation is initially growing but then starts to oscillate once the Jeans mass (that is growing) becomes larger than the mass of the perturbation. This happens earlier for smaller scales. In this phase the magnetic pressure does not play any role, as the much larger radiation pressure is actually providing the force that prevents the collapse. In fact, there is no difference in the evolution parallel and orthogonal to the field, as the radiation pressure is isotropic. The situation changes dramatically after recombination, when the baryon pressure drops and it is instead the magnetic pressure that opposes the growth. However the magnetic pressure can only act in the plane orthogonal to the field. Thus, perturbations in the direction of the field can grow unhindered, while the perturbations that are orthogonal can be stabilized. As it can be seen from Figure 2, this happens basically for all perturbations below the supercluster scale. At $z = 10$, the relative growth of parallel perturbations with respect to orthogonal ones is of order 100, 10 and 3 for the galactic, cluster and supercluster scales, respectively.

The fact that, after recombination, the evolution of the density contrast in the presence of a magnetic field is different

in different directions leads to the reasonable expectation that some degree of anisotropy will be generated even in initially symmetric structures. In order to show this, we consider a Gaussian density fluctuation with standard deviation σ in coordinate space at recombination:

$$\delta(\mathbf{x}, t_{\text{rec}}) = \delta(\mathbf{x} = 0, t_{\text{rec}}) e^{-\frac{|\mathbf{x}|^2}{2\sigma^2}}, \quad (36)$$

where the \mathbf{x} are comoving coordinates centered at the maximum of the perturbation. After Fourier-transforming, we separately evolve the different harmonics in momentum space using Eqs.(24) and we finally transform back to obtain the perturbation in coordinate space at a later time. In Figure 3 we show, for a background magnetic field directed along the y axis and with a present intensity of 1 nGauss, the evolution of a perturbation with $\sigma = 0.5$ kpc at recombination (so that the 3σ region encloses a mass $M \simeq 1.5 \times 10^{11} M_\odot$ at the mean baryonic density, *i.e.*, roughly the mass of a galaxy). In particular, we show equal density contours at $z = 1000, 100$ and 10 . It is evident from the figure how the perturbation becomes progressively squeezed along the direction orthogonal to the magnetic field.

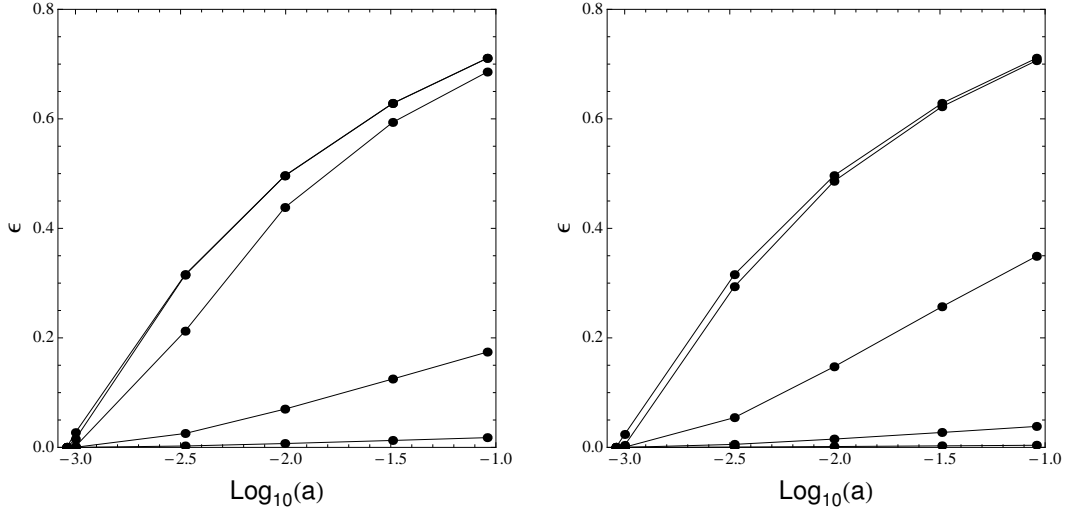


Figure 4: Left panel: Eccentricity ϵ of a Gaussian perturbation at the galactic scale as a function of redshift. The background magnetic field increases by a factor 10 with each curve, starting from $B_0 = 10^{-12}$ G (bottom curve) up to $B_0 = 10^{-9}$ G (top curve). The two upper curves are only distinguishable at large redshifts. Right panel: the same as the left panel, but for a perturbation at the cluster scale.

In order to quantify the anisotropy in the perturbation, we consider the isodensity contour corresponding to half the value at the peak and calculate its eccentricity $\epsilon = \sqrt{1 - b^2/a^2}$, where a and b are the lengths of the semi-major and semi-minor axis of the contour, respectively. In Figure 4, we show how the eccentricity changes with redshift; for the parameters used above, we get $\epsilon \simeq 0.7$ at $z = 10$.

7. Conclusions

We have studied the effect of a background magnetic field on the linear evolution of cosmological density perturbations at scales well below the Hubble length, where a Newtonian treatment can be used, focusing on the matter-dominated era. The conditions that allow the growth of small density perturbations have been clearly stated; in particular, we have found that in the plane orthogonal to the ambient magnetic field, a new critical length appears, related to the presence of the magnetic pressure, while everywhere else outside that plane the stability is dictated by the standard Jeans criterion. This is also confirmed through a direct numerical integration of the relevant MHD equations during the matter-dominated era, where this effect is shown to be possibly important after recombination, when the magnetic pressure is much larger than the kinetic pressure of the residual ionized nuclei. Finally, it has been shown how the dependence of the critical scale on the angle between the perturbation wavevector and the magnetic field could lead to a sizeable anisotropy in the perturbations at the onset of non-linearity.

Our analysis has relied on some approximations: other than those already stated, we have ignored the gravitational effects of dark matter perturbation and we have assumed that after recombination the perturbations in the neutral baryon component trace those in the charged component. We have argued that these approximations limit the validity of our treatment to some

time after recombination. We defer a more detailed and fully general relativistic analysis, also taking into account the different fluid components, to a future work.

Acknowledgment: NC gratefully acknowledges the CPT - Université de la Méditerranée Aix-Marseille 2 and the financial support from “Sapienza” University of Roma. ML acknowledges support from a joint Accademia dei Lincei / Royal Society fellowship for Astronomy.

Appendix A. Hypergeometric Coefficients

In following, we write the complete form of the coefficients of the hypergeometric function of Eq.(28). They read:

$$a_{1(1/2)} = 1 \mp \sqrt{\Delta_-}/12\nu - \sqrt{1 - 36\mu^2\Lambda_2}/12\nu, \quad (\text{A.1a})$$

$$a_{1(3/4)} = 1 \mp \sqrt{\Delta_+}/12\nu - \sqrt{1 - 36\mu^2\Lambda_2}/12\nu, \quad (\text{A.1b})$$

$$a_{2(1/2)} = 1 \mp \sqrt{\Delta_-}/12\nu + \sqrt{1 - 36\mu^2\Lambda_2}/12\nu, \quad (\text{A.1c})$$

$$a_{2(3/4)} = 1 \mp \sqrt{\Delta_+}/12\nu + \sqrt{1 - 36\mu^2\Lambda_2}/12\nu, \quad (\text{A.1d})$$

and

$$b_{1(1/2)} = 1 \mp \sqrt{\Delta_-}/6\nu, \quad (\text{A.2a})$$

$$b_{2(1/2)} = 1 \mp \sqrt{\Delta_-}/12\nu - \sqrt{\Delta_+}/12\nu, \quad (\text{A.2b})$$

$$b_{3(1/2)} = 1 \mp \sqrt{\Delta_-}/12\nu + \sqrt{\Delta_+}/12\nu, \quad (\text{A.2c})$$

$$b_{1(3)} = 1 - \sqrt{\Delta_+}/6\nu, \quad (\text{A.2d})$$

$$b_{2(3)} = 1 - \sqrt{\Delta_-}/12\nu - \sqrt{\Delta_+}/12\nu, \quad (\text{A.2e})$$

$$b_{3(3)} = 1 + \sqrt{\Delta_-}/12\nu - \sqrt{\Delta_+}/12\nu, \quad (\text{A.2f})$$

$$b_{1(4)} = 1 - \sqrt{\Delta_-}/12\nu + \sqrt{\Delta_+}/12\nu, \quad (\text{A.2g})$$

$$b_{2(4)} = 1 + \sqrt{\Delta_-}/12\nu + \sqrt{\Delta_+}/12\nu, \quad (\text{A.2h})$$

$$b_{3(4)} = 1 + \sqrt{\Delta_+}/6\nu. \quad (\text{A.2i})$$

References

- [1] E. Komatsu, et al. [WMAP Collaboration], *Astrophys. J. Suppl.* **192**, 18 (2011).
- [2] D. Larson et al., *Astrophys. J. Suppl.* **192**, 16 (2011).
- [3] J. Dunkley et al., in [arXiv:1009.0866].
- [4] M. Tegmark et al., *Astrophys. J.* **606**, 702 (2004).
- [5] S. Cole et al. [The 2dFGRS Collaboration], *Mon. Not. RAS* **362**, 505 (2005).
- [6] M. Tegmark et al. [SDSS Collaboration], *Phys. Rev. D* **74**, 123507 (2006).
- [7] A.G. Riess et al. [Supernova Search Team Collaboration], *Astron. J.* **116**, 1009 (1998).
- [8] S. Perlmutter et al. [Supernova Cosmology Project Collaboration], *Astrophys. J.* **517**, 565 (1999).
- [9] J. Frieman, M. Turner, D. Huterer, *Ann. Rev. Astron. Astrophys.* **46**, 385 (2008).
- [10] F. Iocco, G. Mangano, G. Miele, O. Pisanti, P.D. Serpico, *Phys. Rept.* **472**, 1-76 (2009).
- [11] D.W. Hogg et al., *Astrophys. J.* **624**, 54 (2005).
- [12] J.D. Barrow, P.G. Ferreira, J. Silk, *Phys. Rev. Lett.* **78**, 3610 (1997).
- [13] D. Paoletti, F. Finelli, *Phys. Rev. D* **83**, 123533 (2011).
- [14] E.S. Scannapieco, P.G. Ferreira, *Phys. Rev. D* **56**, 7493-7497 (1997).
- [15] J. Adamek, R. Durrer, E. Fenu, M. Vonlanthen, *JCAP* **06**, 017 (2011).
- [16] J.D. Barrow, R. Maartens, C.G. Tsagas, *Phys. Rep.* **449**, 131 (2007).
- [17] L. Vlahos, C. Tsagas, D. Papadopoulos, *Astrophys. J.* **629**, L9 (2005).
- [18] C. Tsagas, R. Maartens, *Phys. Rev. D* **61**, 083519 (2000).
- [19] T.V. Ruzmaikina, A.A. Ruzmaikin, *Sov. Astron.* **14**, 963 (1971).
- [20] E.-j. Kim, A. Olinio, R. Rosner, *Astrophys. J.* **468**, 28 (1996).
- [21] N. Carlevaro, G. Montani, *Class. Quant. Grav.* **22**, 4715 (2005).
- [22] N. Carlevaro, G. Montani, *Int. J. Mod. Phys. D* **18**, 1257 (2009).
- [23] N. Carlevaro, G. Montani, *Mod. Phys. Lett. A* **20**, 1729 (2005).
- [24] NRL Plasma Formulary 2009.
- [25] S. Weinberg, *Gravitation and Cosmology* (John Wiley & Sons, 1972).
- [26] S. Weinberg, *Astrophys. J.* **168**, 175 (1971).
- [27] E.W. Kolb, M.S. Turner, *The Early Universe* (Addison-Wesley, 1990).
- [28] G. Montani, M.V. Battisti, R. Benini, G. Imponente, *Primordial Cosmology* (World Scientific, 2011).
- [29] D. Pugliese, N. Carlevaro, M. Lattanzi, G. Montani, R. Benini, submitted to *Physica D*, June 2011.